Crystallite size-dependent optical properties of nanostructured NiO films

S. A. MAKHLOUF[*], M. A. KASSEM, M. A. ABDEL-RAHIM
Department of Physics, Faculty of Science, Assiut University, Assiut 71516, Egypt

Nickel oxide films with different crystallite size were obtained by post annealing of Ni(OH)$_2$ films in air at 523–673 K. The structure, surface morphology and thickness of the as-deposited and annealed films were investigated using XRD, FTIR spectroscopy and SEM. The crystallite size was found to increase with increasing the annealing temperature. Optical absorption study in 200–900 nm wavelength range reveals high absorption for wavelengths less than 400 nm in the UV and visible range. The UV absorption edge of NiO nanostructured films show shorter wavelength-shift that increases with increasing the crystallite size. NiO films exhibit optical transition by both direct and indirect allowed transitions. Direct and indirect optical energy gaps were calculated and found to decrease from 3.25 to 2.87 eV and 3.84 to 3.62 eV respectively; while the width of the localized states increases from 0.306 to 0.586 eV with decreasing the crystallite size from 23.4 to 5.7 nm.

1. Introduction

There has been a great interest in the study of transition metal oxide semiconducting thin films and nanoparticles in the past decades. The most prevailing among them is NiO by virtue of its use in various applications, such as solar cells, solar thermal absorbers, catalyst for O$_2$ evolution, photoelectrolysis, and electrochromic devices [1–4]. NiO is also a well-known material used as positive electrode in batteries. NiO thin films with switching properties suitable for memory devices were successfully deposited by reactive sputtering [5]. Furthermore NiO is an antiferromagnetic (AF) material, and can be used as an AF biasing layer in exchange biased read head devices [6]. NiO films obtained by vacuum deposition and subsequent post-deposition annealing [7] were found to be polycrystalline fcc with the orientation along (111) plane, and needle-like growth were found at initial stages of oxidation mechanism. NiO thin films of various thicknesses have been prepared by RF magnetron sputtering in a pure oxygen atmosphere [8]. The smallest sheet resistance and resistivity have been reported for 200 nm thick films prepared on unheated substrates, whereas the optical transmittance was found to decrease with increasing film thickness [8].

Quantum confinement effects on the properties of a variety of metal oxides have received considerable attention due to enhanced properties such as photoluminescence and electroluminescence as well as variations in the optical band gap. It was found that the optical properties strongly depend on the crystallite sizes [9–15].

Spray pyrolysis (SP) technique has been successfully used to prepare thin films of metal, metal oxides, nanoparticles and composites with controlled composition, morphology, good crystallinity, and uniform size distribution. In this technique, the precursor solution is pulverized by means of compressed gas so that it arrives at the substrate in the form of very fine droplets. Ni and NiO nanoparticles have also been obtained by low-pressure spray pyrolysis (SP) technique [16]. In that study, the effect of preparation parameters including the reducing agent on the size, morphology, and crystallinity of the Ni nanoparticles has been done. It was found that pressure and carrier gas flow rate plays a crucial role in the reduction of NiO to Ni.

In the present work, we have employed the low pressure SP technique to obtain good adherent films of Ni(OH)$_2$ and NiO by post-annealing of Ni(OH)$_2$ films. The prepared films have been investigated for their structural, morphological and optical properties. The crystallinity, molecular structure and morphological studies have been done by using XRD, FTIR and SEM. Optical measurements in the 200–900 nm wavelength range including transmittance and reflectance studies have been performed.

2. Experimental details

Nickel hydroxide precursor was first chemically precipitated as described elsewhere [17]. A portion of the resulting green gel was dried in air at 383 K for about 12 hours for further characterization. Amorphous glass slides (1.3 cm × 1.8 cm) were first ultrasonically cleaned using ethanol. About 60 mL of Ni(OH)$_2$ aqueous solution (0.054

M) was sprayed on the amorphous glass substrates preheated to ~ 343 K. The solution was sprayed in successive intervals to obtain rather uniform films. Ni(OH)$_2$ films thus obtained were annealed at temperatures 473, 523, 573, 623 and 673 K for 3 hours. Five films are obtained and are given code names N$_1$–N$_5$ respectively. XRD patterns are obtained at room temperature using a Philips PW1700 diffractometer equipped with automatic divergent slit, CuK$_\alpha$ radiation and a graphite monochromator (λ = 0.15418 nm). Infrared (IR) spectroscopic study is performed using an IR-470 SHIMADZU infrared spectrophotometer in the range 500–4000 cm^{-1}. Small portions of the samples were collected by scratching the films gently from the glass slides. The scratched portions were mixed finely with KBr in agate mortar and pelletized prior to the measurements. A JEOL JSM-5400 LV scanning electron microscope is used to examine the surface morphology and to measure the thickness of the films by monitoring their cross-sections. Optical absorption is studied by acquiring the reflectance (R) and the transmittance (T) of the as-deposited and post-annealed films in the wavelength range 200–900 nm using a UV-VIS 2101PC scanning spectrophotometer.

3. Results and discussion

3.1 Structural properties

Fig. 1 shows the XRD patterns of the as-deposited Ni(OH)$_2$ and for films annealed at indicated temperatures. Analysis of the diffraction patterns of films annealed at temperatures T $\geq$ 523 K reveals that the formed phase is pure fcc NiO without any observable traces of Ni(OH)$_2$.
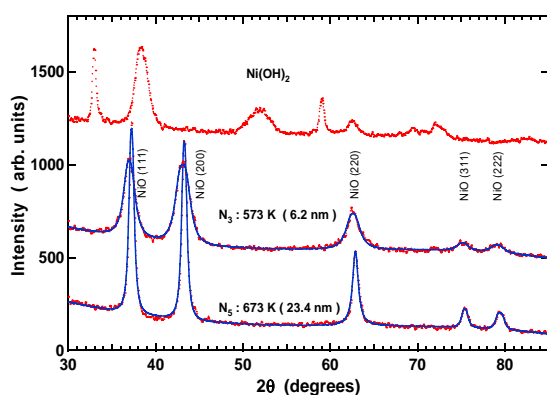
Fig. 1. XRD patterns for as-deposited Ni(OH)$_2$ and post-annealed NiO nanostructured films at the indicated temperatures.

The crystallite size was estimated from x-ray diffraction line broadening using a modified Debye-Scherrer method. Following the same procedure described in ref. [17], the crystallite size of the present nanostructured NiO films was found to increase from 5.7

to 23.4 nm with increasing the annealing temperature from 523 to 673 K.

Fig. 2 shows the FTIR spectra for the as deposited Ni(OH)$_2$ and NiO films obtained by post-annealing at different temperatures. An upward offset of 20 units is made for the spectrum of N$_5$ film for clarity purposes. As shown in Fig. 2, the spectrum of Ni(OH)$_2$ film shows its characteristic bands. A sharp band is found at 3650 cm^{-1}, which is characteristic for stretching vibration ν(OH) exists in non-hydrogen bonded OH groups and indicates strongly β-Ni(OH)$_2$ existence [18]. The broad band around 3430 cm^{-1} is due to the stretching ν(OH) exists in hydrogen bonded groups originate from Ni(OH)$_2$ sheets and from water adsorption [19–21]. The intense band centered at 1630 cm^{-1} is due to the bending vibration δ(OH) of the absorbed water molecules on the surface of the powder particles [18–23]. The overlapping bands at 1380 – 1400 cm^{-1} are thus due to both ionic and covalent bonds of resident nitrates [22]. From the above analysis one can say that the as-deposited film could be described as hydrated and less crystallized β-Ni(OH)$_2$. XRD pattern of the as-deposited film, shown in Fig. 1, is characteristic of the β-Ni(OH)$_2$ phase and shows no peaks for the α-phase. The spectrum of N$_2$ film which is calcined at 523 K indicates incomplete decomposition of Ni(OH)$_2$. Thermal gravimetric analysis TGA was performed, is not presented here, for a portion of the Ni(OH)$_2$ powder and indicated that decomposition of Ni(OH)$_2$ starts at ~493 K and ends at ~573 K. Films post-annealed at temperatures $\geq$ 573 K give spectra with broad and relatively weak bands only around 1610, 2930 and 3450 cm^{-1} indicating that these films are less hydrated NiO.
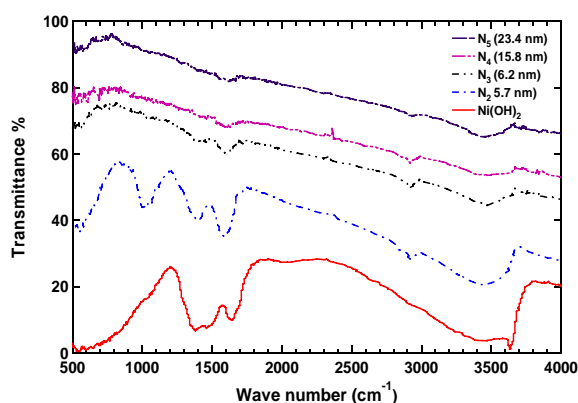
Fig. 2. IR transmittance spectra of as-deposited Ni(OH)$_2$ and post-annealed NiO powders scratched from the slides.

Fig. 3 shows SEM images for the as-deposited Ni(OH)$_2$, N$_3$ and N$_5$ films. Fig. 3d shows the cross-section of N$_2$ film indicating ~ 10 μm in thickness. The annealed films are more homogeneous and less porous than the as-deposited one. Annealing at temperatures higher than 673 K produces films with rather inhomogeneous thickness.

Such inhomogeneity in the thickness of films may be due to the softness of the glass substrates and hence partial diffusion of the material through the glass at such high temperatures [24].
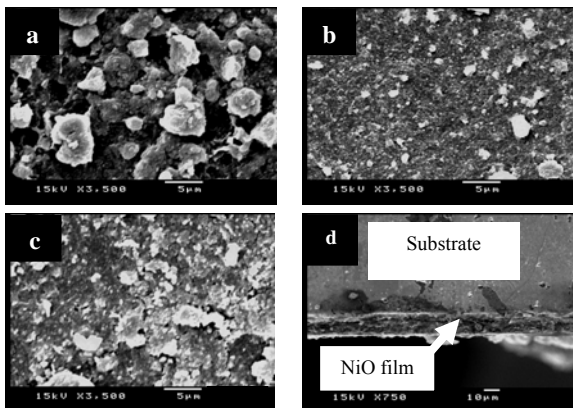
Fig. 3. SEM images for as-deposited Ni(OH)₂ (a), N₃ (b), N₅ (c) and a cross-section of N₂ film (d).

3.2 Optical properties

The transmittance $T (\lambda)$ and the reflectance $R (\lambda)$ spectra for normal incident light in the wavelength range 200–900 nm of as-deposited Ni(OH)$_2$ and nanostructured NiO films of different crystallite size are shown in Figs. 4a and 4b, respectively. It can be noted that the Ni(OH)$_2$ film is more transparent and less reflecting than NiO films. Transmittance and reflectance spectra of N$_1$ film are very close to those of Ni(OH)$_2$ film, which emphasizes that Ni(OH)$_2$ is not decomposed yet at 473 K. The N$_2$ film with crystallite size ~ 5.7 nm exhibits a drastic decrease in the transmittance. Increasing the crystallite size above 5.7 nm raises the transmittance again over the whole considered range of wavelength. The rapidly decrement of the transmittance with decreasing the wavelength λ below 400 nm indicates high absorption in the UV region. It is noted that the summation of transmittance $T (\lambda)$ and reflectance $R (\lambda)$ in the visible light region, beyond the absorption region is slightly less than unity. This can be related to the loss of some incident photons by scattering on the rough surfaces of the formed films [24].

The absorption coefficient $\alpha (\lambda)$ was computed from the transmittance $T (\lambda)$ and the reflectance $R (\lambda)$ using the relation [25],

$$T(\lambda) = \left[1 - R(\lambda)\right]^2 e^{-\alpha (\lambda)d}, \qquad (1)$$

where d is the film thickness. The optical density (OD = αd) spectra of NiO films of different crystallite size are shown in Fig. 5. All samples show high absorption in the UV region and the absorption edge is shifted to the shorter wavelengths, higher energies, with increasing the crystallite size. The high absorption in a semiconductor occurs for photons of energy (hν) sufficient for electronic transitions, i.e. photons of energy in the order of the

energy gap E$_g$ of the semiconductor. The values of E$_g$ is related to the existence of localized states in the forbidden energy gab [26]. These localized states are associated with the defects and the unsaturated bonds in the lattice. Defects in NiO bulk crystals originate from the existence of a less stoichiometric high conductivity surface layer of thickness about 50 atomic layers [27]. In the present nanostructured films, the surfaces of the grains contain high concentration of Ni^{++} vacancies which correspond to an acceptor like level in the forbidden energy gap just above the 3d localized state of Ni^{2+} and 2p wide band of O^{2-} and close to the Fermi level [28]. Ni^{++} vacancies are produced because the oxygen ions can not be incorporated in the NiO lattice. For each Ni^{++} vacancy two adjacent Ni^{2+} ions combine to form Ni^{3+} ion acquiring charge neutrality and hence result in a lattice distortion [29]. This change in the oxidation state of nickel in the lattice is the origin of the observed high absorption in the UV and visible range [30,31]. Increasing the annealing temperature and hence the crystallite size, Ni^{3+} ions are removed [22] and the defects are reduced resulting in the observed shift to the shorter-wavelengths.
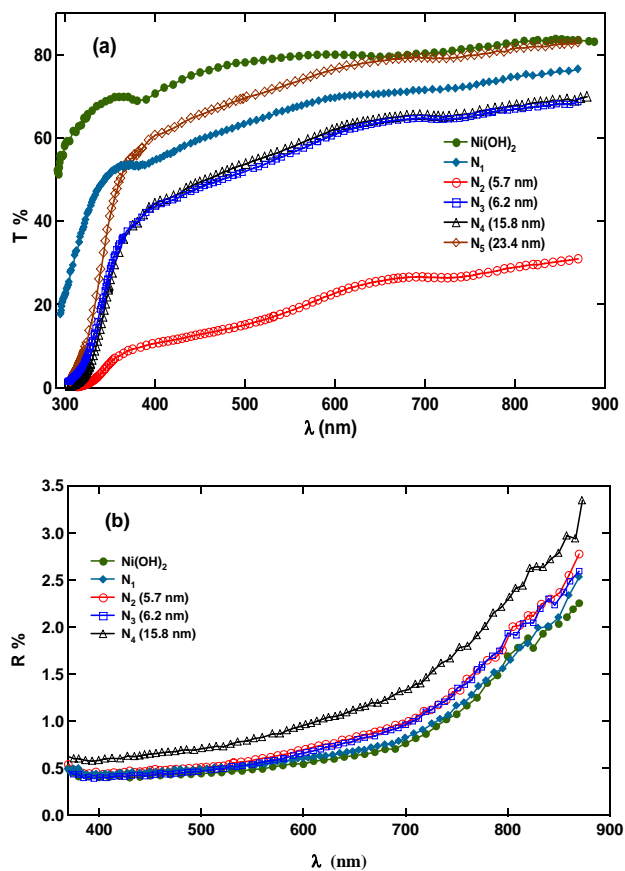
Fig. 4. Transmittance spectrum (a) and reflectance spectrum (b) of the as-deposited nickel hydroxide and NiO nanostructured films of different crystallite size.

Fig. 5 indicates that the behavior of α *vs.* $h\nu$ can be divided into two regions: the exponential edge region and

the high absorption region. In the exponential region, the absorption coefficient α obeys Urbach's relation [32],

$$\alpha = \alpha_o e^{h\nu/E_e} \quad , \qquad (2)$$

where α_o is a constant and E_e is the width of the localized states in the forbidden energy gap.
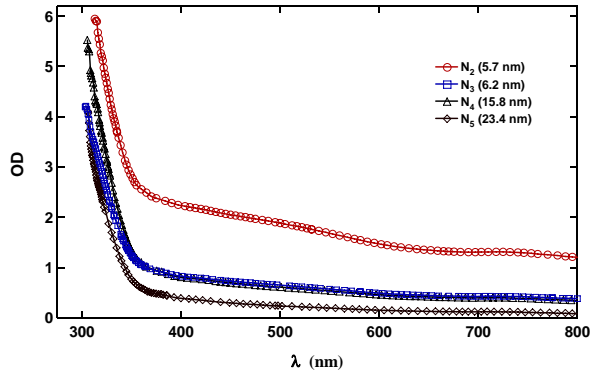
Fig. 5. Optical density (OD) spectra for nanostructured NiO films at indicated crystallite size.

The values of the localized states width E_e are obtained from *log α vs. hν* plots in the exponential edge region as shown in Fig. 6. The obtained values of E_e decrease from 0.586 to 0.306 eV with increasing the crystallite size from 5.7 to 23.4 nm as shown in Fig. 8.
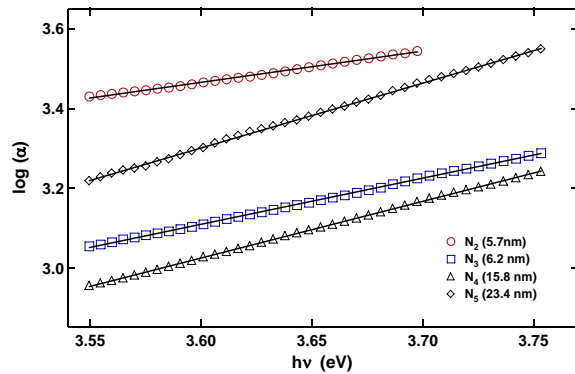
Fig. 6. log (α) as a function of hν for the NiO nanostructured films. Solid lines are the linear fits.

The behavior of E_e with the crystallite size emphasizes the effect of the annealing temperature on removing Ni^{3+} ions and decreasing the defects in the NiO lattice [22]. On the other hand and in the high absorption region, α is related to the incident photon energy *hν* by:

$$\alpha h\nu = C\left(h\nu - E_g\right)^r \quad , \qquad (3)$$

where C is a constant. The exponent r determines the nature of electronic transition and E_g is the energy band gab. The best fitting for this equation was found for $r = 2$

and $r = 1/2$ indicating that the photons induce electronic transition by both indirect and direct allowed transition, respectively. The indirect transition energy E_g^{ind} is determined by extrapolating the linear parts of $(\alpha h\nu)^{1/2}$ vs. *hν* plots to $\alpha = 0$ as shown in Fig. 7a. The direct transition energy E_g^{dir} is determined from $(\alpha h\nu)^2$ vs. *hν* plots by the same manner, as shown in Fig. 7b. Fig. 8 indicates that the indirect energy gap increases monotonically with the crystallite size from 2.87 to 3.25 eV whereas the direct energy gap increases from 3.62 to 3.84 eV with increasing the crystallite size from 5.7 to 23.4 nm.
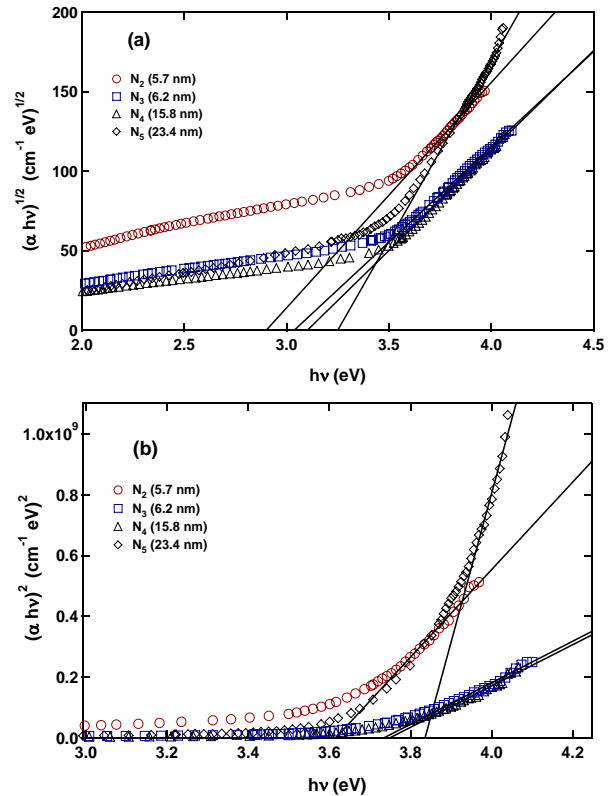
Fig. 7. The dependence of $(\alpha h\nu)^{1/2}$ (a) and $(\alpha h\nu)^2$ (b) on hν for NiO films at indicated crystallite size. Solid lines are the linear fits.

This can be attributed to the reduction of the defects in NiO lattice with increasing crystallite size. The removal of Ni^{3+} ions decreases the density of the localized states tails in the band structure and consequently decreases the width of the localized states and increases the optical energy gap. The obtained values of the direct and indirect energy gaps, and the width of the localized states are in good agreement with those reported for NiO films prepared by various techniques [22,24,33−35]. The variation of direct and indirect E_g with crystallite size is consistent with the reported variation of the activation energy for conduction with particle size as reported for NiO nanoparticles [17]. Occasionally films annealed at temperatures higher than

673 K exhibit unsystematic optical properties, which can be ascribed to the inhomogeneous thickness.

The refractive index (n) is related to the optical reflectance and the extinction coefficient (k) by:

$$R = \frac{(n-1)^2 + k^2}{(n+1)^2 + k^2} , \qquad (4)$$

where k is related to the absorption coefficient α and the wavelength λ by Lambert's law such as,

$$k = \frac{\alpha \, \lambda}{4 \, \pi} , \qquad (5)$$
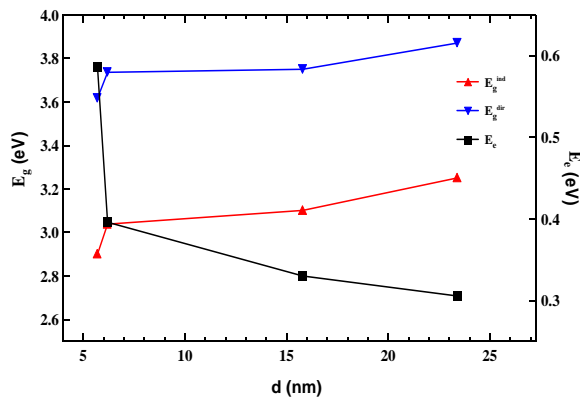
Fig. 8. The crystallite size dependence of the indirect, direct optical energy gap and the width of the localized states of NiO nanostructured films.
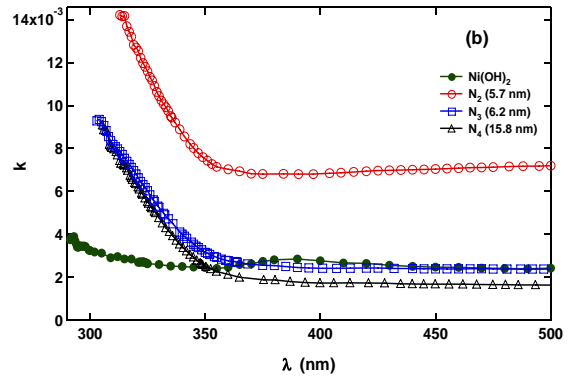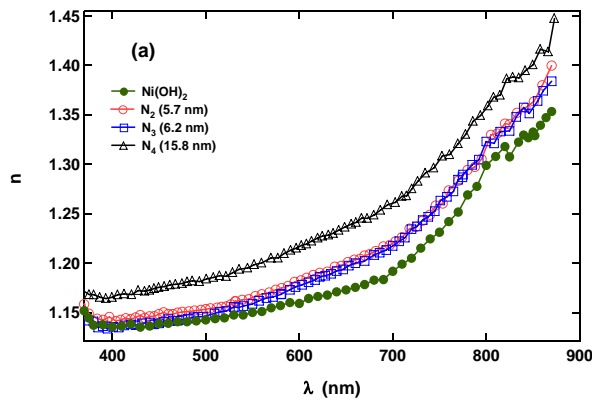
Fig. 9. The dispersion spectra (a) and absorption spectra (b) of as-deposited Ni(OH)₂ and NiO films of different crystallite size.

The spectra of n and k of the as-deposited Ni(OH)$_2$ and NiO nanostructured films are presented in Figs. 9a and 9b, respectively. Both n and k of the as-deposited Ni(OH)$_2$ are less than those of NiO nanostructured films. For NiO nanostructured films, increasing the crystallite size increases n but decreases k, which can be also attributed to the decrease of the defects in the NiO lattice as the crystallites grow. It should be noted that our samples exhibits an anomalous dispersion in the wavelength range of measurement. The real part (ε_1) and imaginary part (ε_2) of the dielectric constant for as-deposited Ni(OH)$_2$ and NiO nanostructured films can be calculated from n and k [36] using:

$$\varepsilon_1 = n^2 - k^2 , \qquad (6)$$

$$\varepsilon_2 = 2nk , \qquad (7)$$

The behavior of both ε_1 and ε_2 with the wavelength is presented in Figs. 10a and 10b, respectively. As shown ε_1 increases and ε_2 decreases with increasing the wavelength and both ε_1 and ε_2 of NiO films are greater than those of the as-deposited Ni(OH)$_2$ film. Increasing the crystallite size increases ε_1 in the wavelength range of measurement. It should be mentioned that the behavior of ε_1 of consolidated NiO nanoparticles with the frequency in the range 1-100 kHz was studied electrically and reported elsewhere [17]. Nanostructured NiO films, in the UV and visible light region, and consolidated NiO nanoparticles, in the long waves region, exhibited the same variation of the real part of the dielectric constant with the frequency.
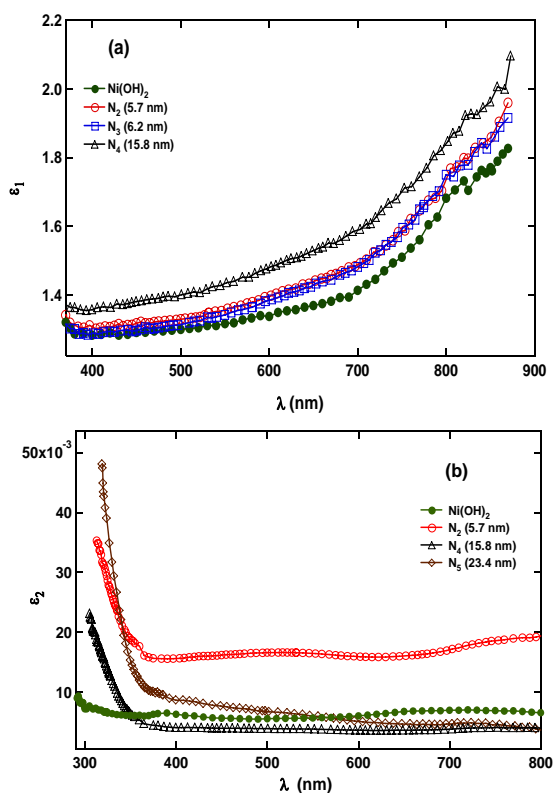
Fig. 10. Variation of ε₁ (a) and ε₂ (b) of as-deposited Ni(OH)₂ and NiO films of different crystallite size with the wavelength λ.

4. Conclusion

In conclusion, nanostructured NiO films were obtained by post-annealing of Ni(OH)₂ films and were characterized using various techniques. The crystallite size increases from 5.7 to 23.4 nm with increasing the annealing temperature from 523 to 673 K. Optical absorption study revealed high absorption of nanostructured NiO films in the UV region. The absorption edge shows a shorter wavelength-shift that increases with increasing the crystallite size. Optical transition occurs via both direct and indirect allowed transitions. Direct and indirect optical energy gaps decreases, whereas the width of the localized states increases with decreasing the crystallite size.

References

[1] J. G. Cook, F. P. Koffyberg, Solar Energy Mater. **10**, 55 (1984).
[2] J. C. N. Botejue, A. C. C. Tseung, J. Electrochem. Soc. **132**, 2957 (1985).
[3] F. P. Koffyberg, F. A. Benko, J. Electrochem. Soc. **128**, 2476 (1981).
[4] H. Kamal, E. K. Elmaghraby, S. A. Ali, K. Abdel-Hady, Thin Solid Films **483**, 330 (2005).
[5] J. W. Lee, I. H. Park, C. W. Chung, Integrated ferroelectrics **74**, 71 (2005).
[6] E. Fujii, A. Tomozawa, H. Torii, R. Takayama, Jpn. J. Appl. Phys. **35**, 328 (1996).
[7] B. Sasi, K. G. Gopchandran, P. K. Manoj, P. Koshy, P. Prabhakara Rao, V. K. Vaidyan, Vacuum **68**, 149 (2003).
[8] H. L. Chen, Y. M. Lu, W. S. Hwang, Thin Solid Films **514**, 361 (2006).
[9] B. M. Tissue, Chem. Mater. **10**, 2837 (1998).
[10] M. I. Freedho, A. P. Marchetti, Interfaces and Surfaces, in Handbook of Optical Properties Volume II Optics of Small Particles, CRC Press, New York (1997).
[11] R. J. Gehr, R. W. Boyd, Chem. Mater. **8**, 1807 (1996).
[12] Y. Kanemitsu, Phys. Rep. **263**, 1 (1995).
[13] A. D. Yoffe, Adv. Phys. **42**, 173 (1993).
[14] I. Kosacki, V. Petrovsky, H. U. Anderson, Appl. Phys. Lett. **74**, 341 (1999).
[15] M. G. Krishna, A. K. Bhattacharya, Int. J. Mod. Phys. B **15**, 191 (2001).
[16] W. N. Wang, Y. Itoh, I. Wuled Lenggoro, K. Okuyama, Mater. Sci. Eng. B **111**, 69 (2004).
[17] S. A. Makhlouf, M. A. Kassem, M. A. Abdel-Rahim, J. Mater. Sci. 44, 3438 (2009).
[18] P. Oliva, J. Leonardi, J. F. Laurent, C. Delmas, J. J. Braconnier, M. Figlarz, F. Fievet, A. de Guibert, J. Power Sources **8**, 229 (1982).
[19] F. Flevet, M. Flglarz, J. Catal. **39**, 350 (1975).
[20] C. Barriga, J. M. Fernandez, M. A. Ulibarri, F. M. Labajos, V. Rives, J. Solid State Chem. **124**, 205 (1996).
[21] P. Vishnu Kamath, G. Helen Annal Therese, J. Gopalakrishnan, J. Solid State Chem. **128**, 38 (1997).
[22] A. Mendoza-Galván, M. A. Vidales-Hurtado, A. M. López-Beltrán, Thin Solid Films **517**, 3115 (2009).
[23] S. Deabate, F. Fourgeot, F. Henn, Ionics **5**, 371 (1999).
[24] H. Kamal, E. K. Elmaghraby, S. A. Ali, K. Abdel-Hady, J. Crys. Gro. **262**, 424 (2004).
[25] H. Sakata, K. Hamano, J. Phys. Soc. Jpn. **61**, 3786 (1992).
[26] N. F. Mott, Philos. Mag. **19**, 835 (1969).
[27] M. A. Wittenauer, L. L. Van Zandt, Philos. Mag. B **46**, 659 (1982).

[28] V. Biju, M. Abdul Khadar, Mater. Res. Bull. **36**, 21 (2001).
[29] D. Adler, J. Feinleib, Phys. Rev. B **2**, 3112 (1970).
[30] K. M. E. Miedzinska, B. R. Hollebone, J. G. Cook, J. Phys. Chem. Solids **49**, 1355 (1988).
[31] R. Newman, R. M. Chrenko, Phys. Rev. **114**, 1507 (1959).
[32] F. Urbach, Phys. Rev. **92**, 1324 (1953).
[33] S. A. Mahmoud, A. A. Akl, H. Kamal, K. Abdel-Hady, Physica B **311**, 366 (2002).
[34] P. S. Patil, L. D. Kadam, Appl. Surf. Sci. **199**, 211 (2002).
[35] P. Puspharajah, S. Radhakrishna, A. K. Arof, J. Mater. Sci. **32**, 3001 (1997).
[36] A. Abu El-Fadl, M. M. Hafiz, M. M. Wakaad, A. S. Aashour, Rad. Phys. Chem.**76**, 61(2007).

_____
[*]Corresponding author: smakhlouf@assiut.edu.eg;
                        smakhlouf2@yahoo.com